Electronic Supplementary Information for:

Graphene Oxide in Carbon Nitride: From Easily Processed Precursors to a Composite Material with Enhanced Photoelectrochemical Activity and Long-term Stability

Guiming Peng,‡[a,b] Jiani Qin,‡[a] Michael Volokh,[a] Chong Liu[b] and Menny Shalom*[a]

[a] Department of Chemistry and Ilse Katz Institute for Nanoscale Science and Technology, Ben-Gurion University of the Negev, Beer-Sheva 8410501, Israel.

[b] Institute for Molecular Engineering, University of Chicago, Chicago, Illinois 60637, USA.

‡Authors with equal contribution

*E-mail: mennysh@bgu.ac.il

Experimental characterization

The morphology of the samples was examined by scanning electron microscopy (SEM, JEOL JSM-7400F equipped with a FEG source, operated at 3.5 kV). X-ray diffraction (XRD) patterns were collected using PANalytical's Empyrean diffractometer. X-ray photoelectron spectroscopy (XPS) was collected on Thermo Fisher Scientific ESCALAB 250 using monochromated Kα X-rays (1486.6 eV). Fourier transform infrared spectroscopy (FTIR) was collected using a Thermo Scientific Nicolet iN 10Mx infrared microscope. UV-vis spectra were obtained using a Cary 100 spectrophotometer. Fluorescence measurements were collected using an Edinburgh instruments FLS920P Fluorimeter. Viscosity measurements were performed on an AR 2000 Rheometer (from TA Instruments) at room temperature. Gas chromatography (GC) data was collected using an Agilent 6850 GC equipped with an Agilent HP5-MS column.

Fig. S1 Photographs of melamine paste and melamine/GO pastes with different GO amounts (from $x = 0$ to $x = 0.75$) at preparation (top row) and after 5 days (bottom row).

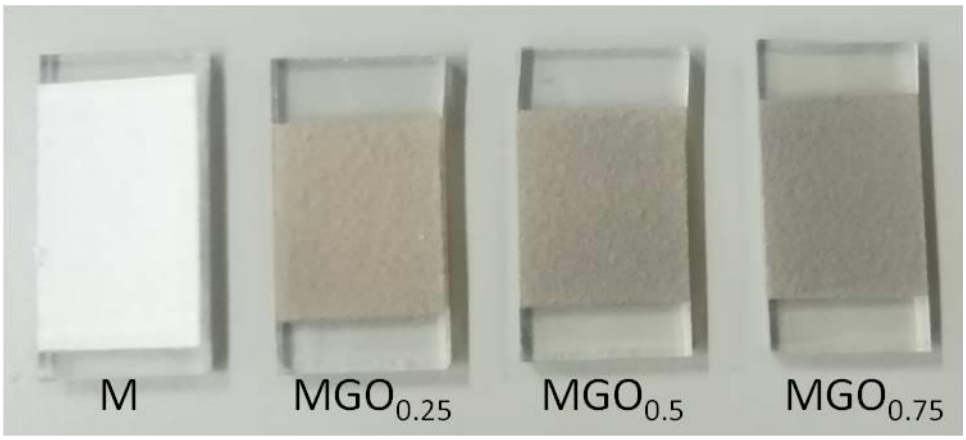

Fig. S2 Photograph of a melamine film (M) and melamine/GO films (MGO_x) on FTO before calcination.

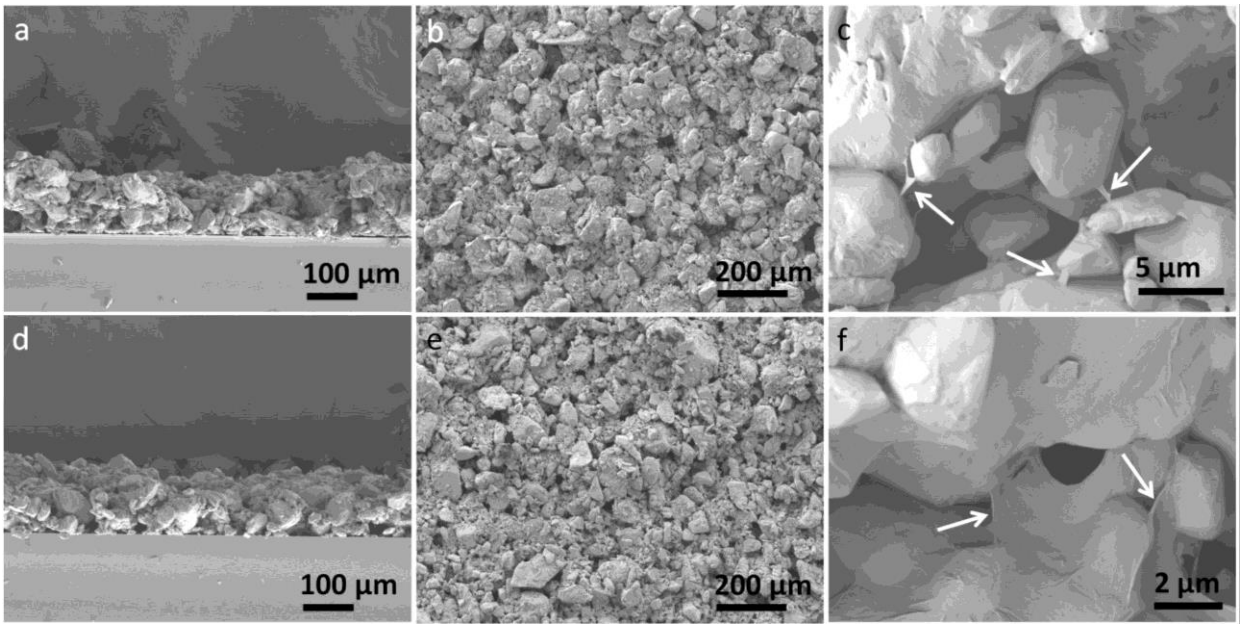

Fig. S3 (a–c) SEM images of $MGO_{0.25}$. (d–f) SEM images of $MGO_{0.75}$. The arrows indicate the presence of GO.

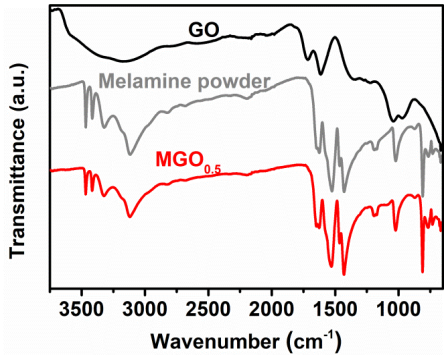

Fig. S4 FTIR spectra of GO, melamine powder (pristine), and $MGO_{0.5}$ film.

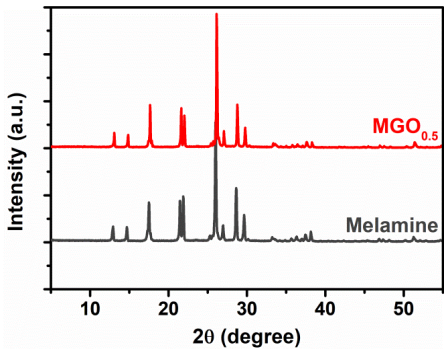

Fig. S5 XRD patterns of melamine and $MGO_{0.5}$ films.

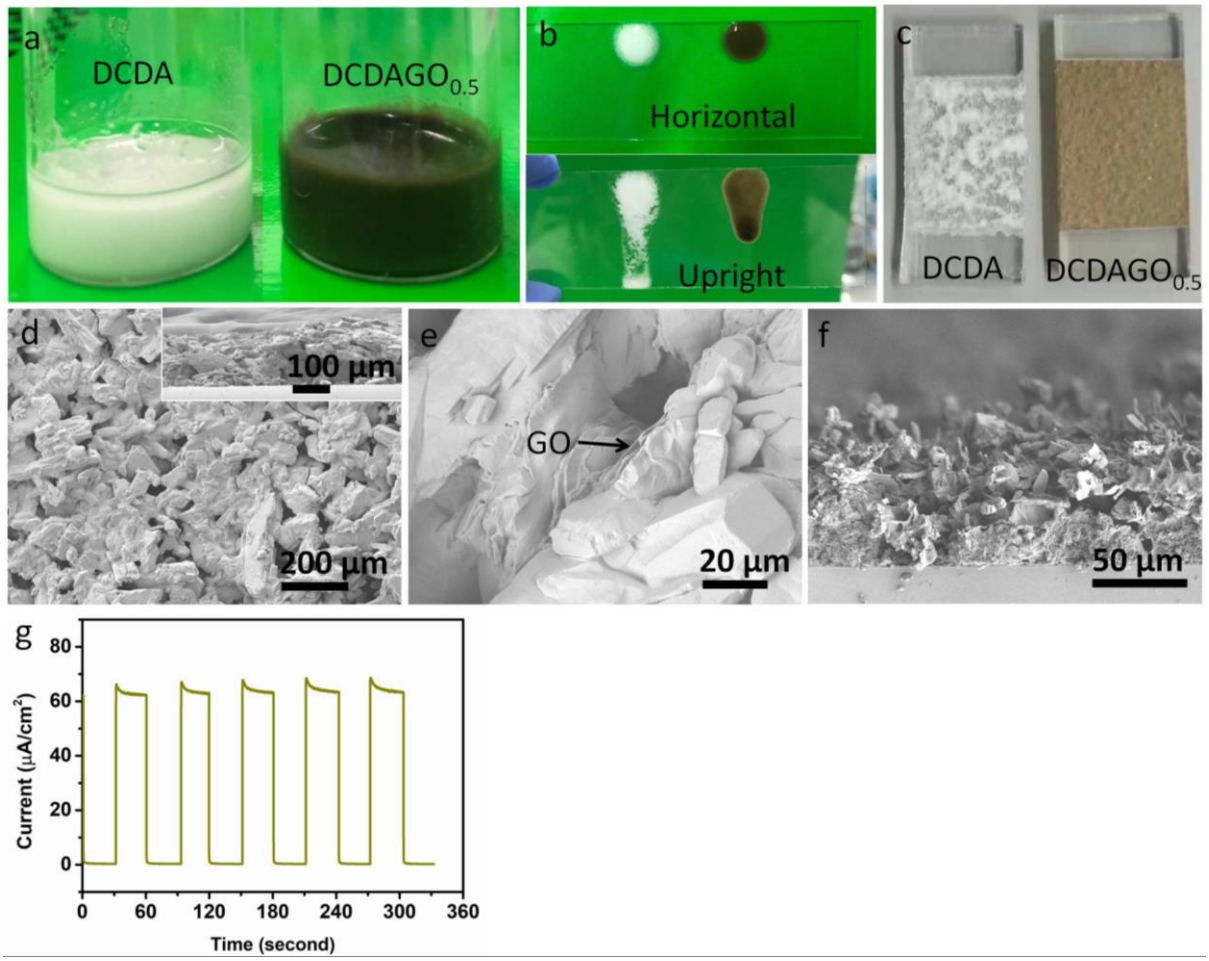

Fig. S6 (a) Photographs of dicyandiamide paste (DCDA) and dicyandiamide/$GO_{0.5}$ paste ($DCDAGO_{0.5}$). (b) Photographs of a fluidity test on glass slide. (c) Photographs of DCDA and $DCDAGO_{0.5}$ films on FTO. (d, e) SEM images of the $DCDAGO_{0.5}$ film. (f) SEM image of the CN/rGO film after calcination of $DCDAGO_{0.5}$ under N_2 atmosphere at 550 °C for 4 h. (g) Photocurrent of the $CN/rGO_{0.5}$ electrode under one-sun illumination in 0.1 M KOH, which was prepared by calcination of $DCDAGO_{0.5}$.

It is noted that a viscous paste cannot be prepared using DCDA only. Similarly, DCDA suspension cannot be coated onto FTO to form a uniform layer (Fig. S6a–b). However, after the addition of GO, the viscosity is increased (manifested in slower flow rate shown in Fig. S6b), and

the coating ability is greatly improved (Fig. S6c). GO nanosheets can be observed embedded within the DCDA microcrystals (Fig. S6e), speaking for its binder role in DCDA preparation. After thermal condensation, CN/rGO film can be obtained. The SEM image shows that the CN/rGO film is composed of a continuous CN layer on FTO, while on the top surface there are standing microstructures (Fig. S6f). The corresponding electrode after calcination generated a photocurrent of 63.8 μA cm^{-2} under one-sun illumination (Figure S6g).

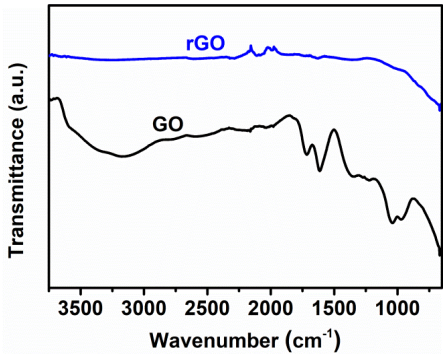

Fig. S7 FTIR spectra of GO and the reduced graphene oxide (rGO) obtained by thermal reduction of GO at 550 °C for 4 h under N_2. Clearly, most of the oxygen-containing functionalities (-OH, C=O, and C-O-C) are removed after the thermal treatment, showing that the GO is reduced to rGO using this method.

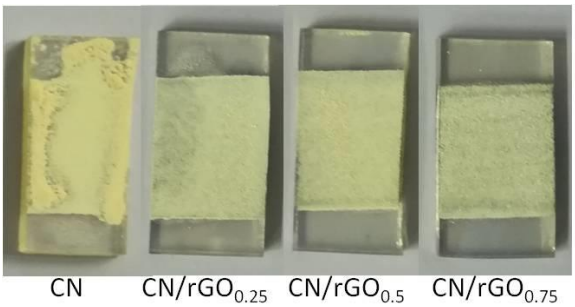

Fig. S8 Photographs of the CN and CN/rGO$_x$ (x = 0.25, 0.5, 0.75) electrodes.

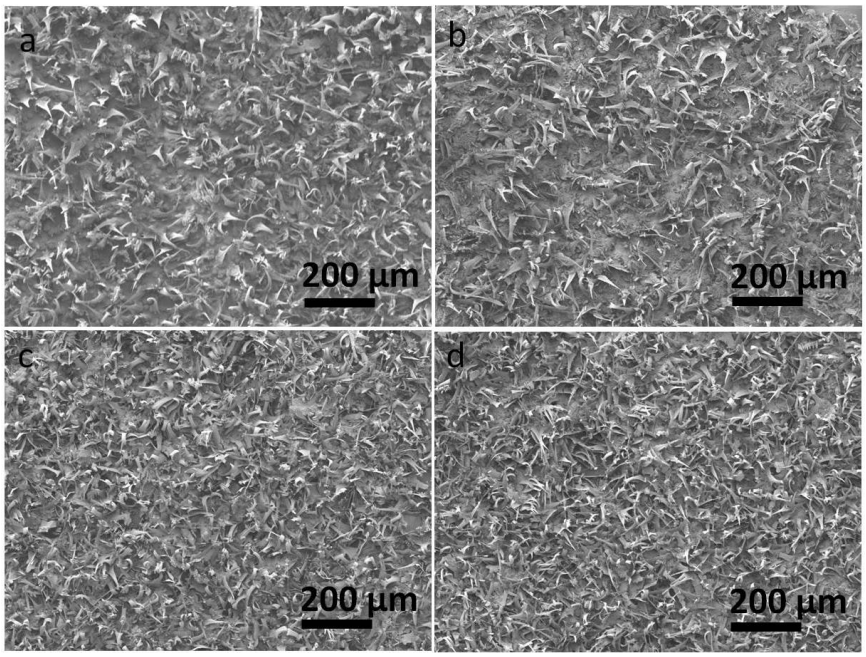

Fig. S9 Top-view SEM images of (a) CN, (b) CN/rGO$_{0.25}$, (c) CN/rGO$_{0.5}$, and (d) CN/rGO$_{0.75}$.

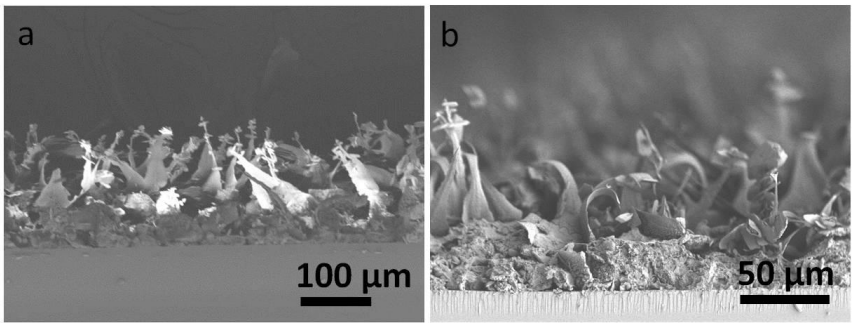

Fig. S10 Cross-sectional SEM image of (a) CN, and (b) CN/rGO$_{0.5}$ electrodes (on FTO).

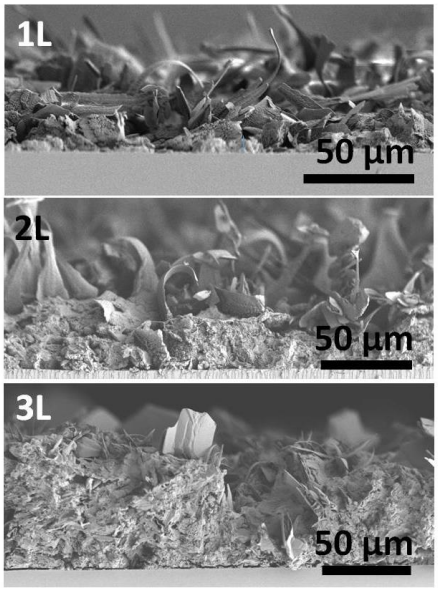

Fig. S11 $CN/rGO_{0.5}$ films of different thickness prepared by 1, 2, and 3 scotch tape layers during doctor-blade coating process. The number of scotch tape layers is indicated on each image. The thickness of the bottom continuous layers is ~7, ~23, and ~57 µm, respectively.

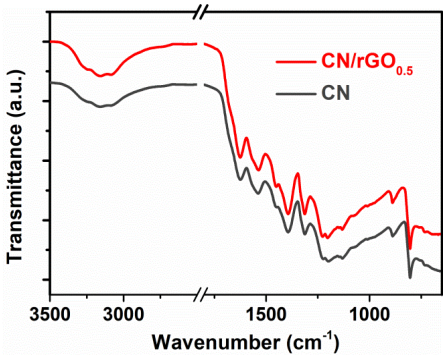

Fig. S12 FTIR spectra of CN and $CN/rGO_{0.5}$.

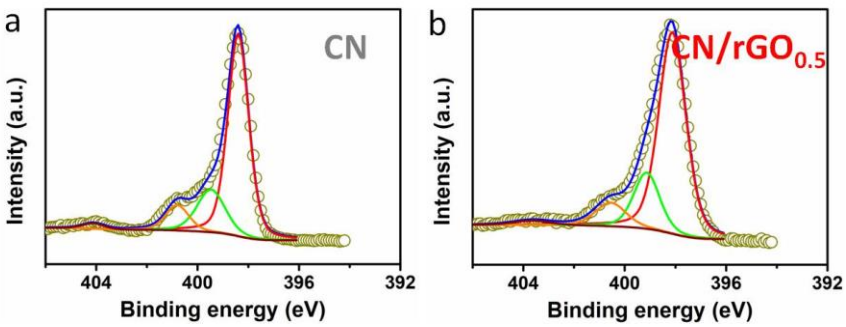

Fig. S13 N1s XPS of (a) CN, and of (b) CN/rGO$_{0.5}$.

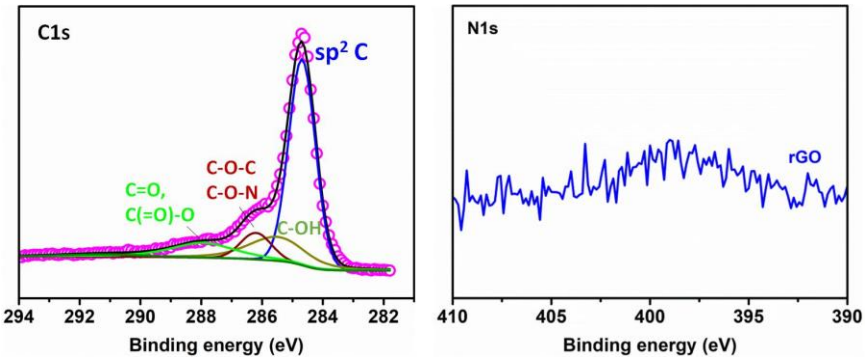

Fig. S14 C1s and N1s XPS spectra of rGO (after the same thermal process of the rGO-containing electrodes).

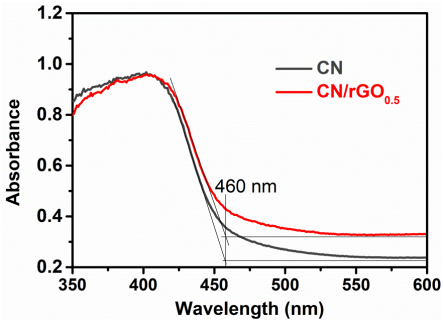

Fig. S15 UV-vis spectra of CN and CN/rGO$_{0.5}$.

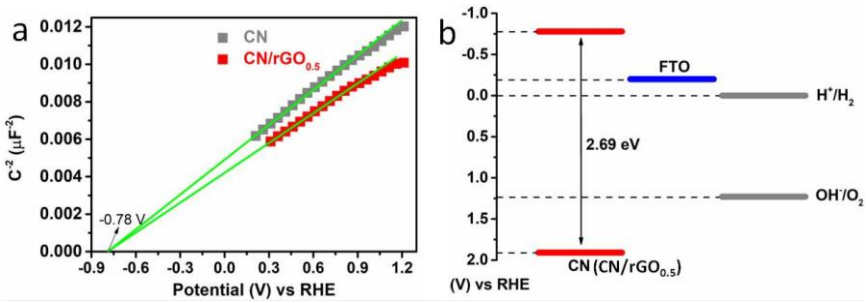

Fig. S16 (a) Mott-Schottky plots, and (b) proposed bandgap diagram of the CN and CN/rGO$_{0.5}$ electrodes.

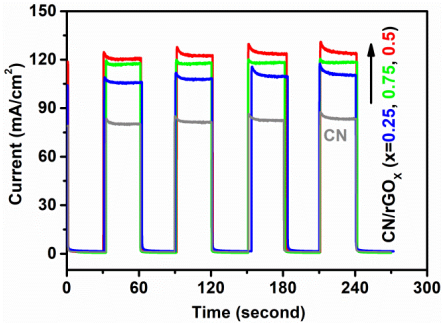

Fig. S17 Photocurrents of CN and CN/rGO$_x$ electrodes at 1.23 V *vs.* RHE in 0.1 M KOH aqueous solution upon cycling on/off 1-sun illumination (chronoamperometry).

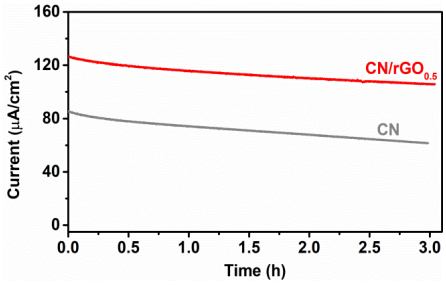

Fig. S18 Photocurrents of CN and CN/rGO$_{0.5}$ electrodes at 1.23 V *vs.* RHE in 0.1 M KOH aqueous solution during 3 h continuous 1-sun illumination.

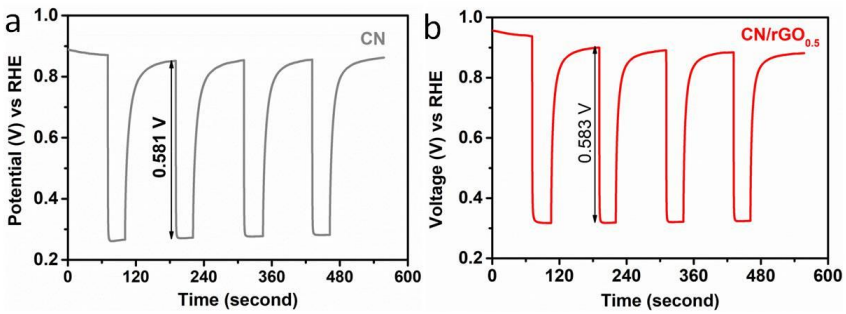

Fig. S19 Open circuit potential of (a) CN electrode and (b) CN/rGO$_{0.5}$ electrode.

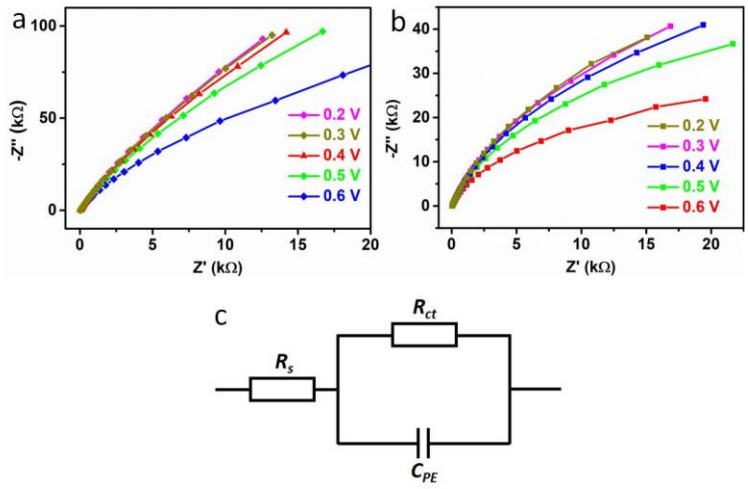

Fig. S20 Nyquist plots of (a) CN, and (b) CN/rGO$_{0.5}$ at different potentials (*vs.* Ag/AgCl) in 0.1 M KOH aqueous solution. (c) The equivalent circuit for the fitting of Nyquist plots.

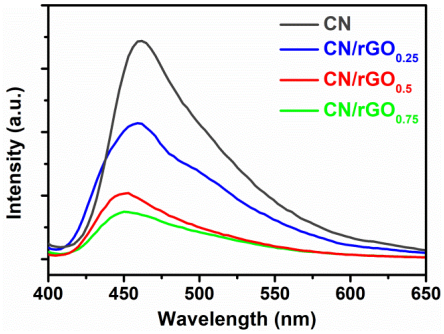

Fig. S21 Fluorescence spectra of CN, CN/rGO$_{0.25}$, CN/rGO$_{0.5}$, and CN/rGO$_{0.75}$. The excitation wavelength is 370 nm.

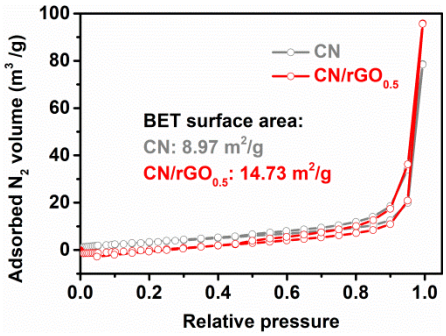

Fig. S22 N_2 adsorption-desorption isotherms plots of the CN and CN/rGO$_{0.5}$ powder scratched from the electrodes. Calculated BET surface areas are 8.97 m^2 g^{-1} and 14.73 m^2 g^{-1} for the CN and CN/rGO$_{0.5}$, respectively.

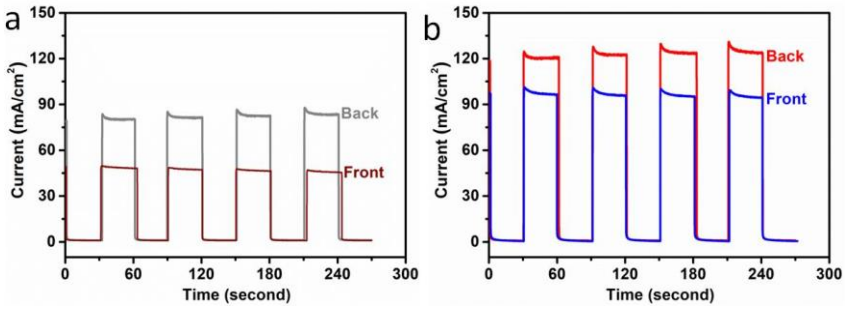

Fig. S23 Photocurrent densities when illuminated from front- and back-side of (a) CN, and (b) CN/rGO$_{0.5}$ electrodes at 1.23 V *vs.* RHE in 0.1 M KOH.

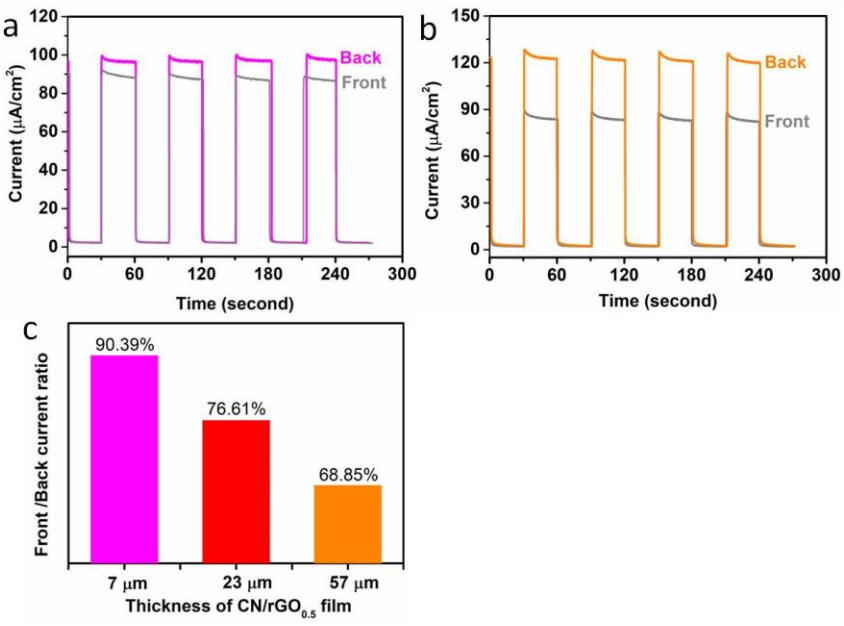

Fig. S24 Photocurrent densities when illuminated from front and back side of $CN/rGO_{0.5}$ electrodes with different thicknesses at 1.23 V *vs.* RHE in 0.1 M KOH. (a) Chronoamperometry of 7 μm thick electrode, (b) Chronoamperometry of 57 μm thick electrode. (c) The ratios of the photocurrent when illuminated from the frontside relative to illumination from the backside of $CN/rGO_{0.5}$ electrodes of each thickness.

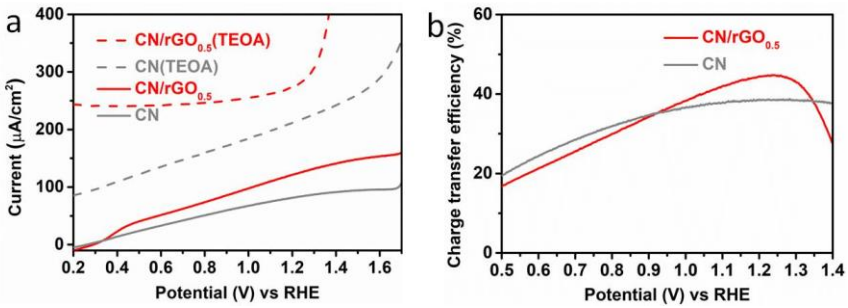

Fig. S25 LSV curves of the CN and $CN/rGO_{0.5}$ electrodes in 0.1 M KOH (solid lines) and 0.1 M KOH aqueous solutions containing 10% (v/v) TEOA (dashed lines) as a hole scavenger. (b) The charge transfer efficiency (defined as the ratio between the photocurrent in 0.1 M KOH divided and that in 0.1 M KOH containing the hole scavenged) plots of CN and $CN/rGO_{0.5}$ electrodes. The hole scavenger used is 10% (v/v) TEOA (triethanolamine, 99%, Carl Roth) in 0.1 M KOH aqueous solution.

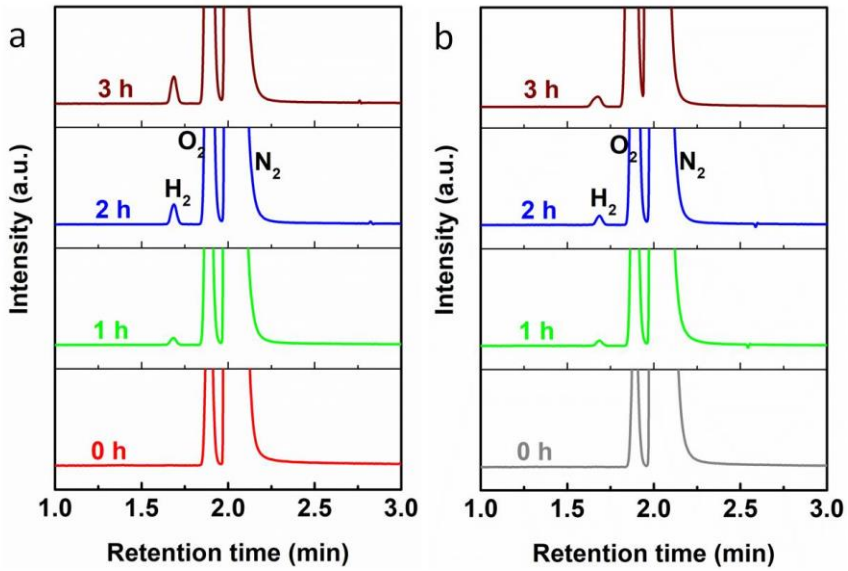

Fig. S26 Gas chromatograms after different photoelectrochemical measurement durations (0, 1, 2, and 3 h) when using (a) $CN/rGO_{0.5}$ and (b) CN as the photoelectrocatalyst under constant 1-sun

illumination. The electrodes are biased at 1.23 V *vs.* RHE, while the electrolyte is 0.1 M KOH containing 10% (v/v) TEOA.

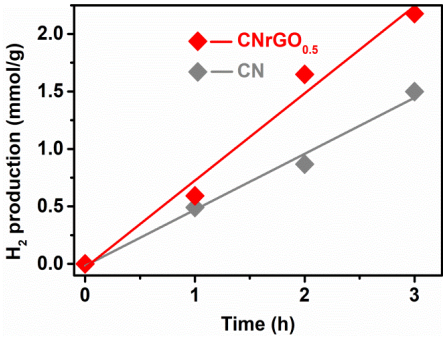

Fig. S27 H_2 production as a function of time.

Table S1. Elemental composition of the CN and CN/$rGO_{0.5}$ obtained by XPS measurements.

Sample	C (atom%)	N (atom%)	O (atom%)	C/N atomic ratio
CN	43.89	55.27	0.84	0.79
CN/$rGO_{0.5}$	44.55	46.65	8.8	0.95

Table S2. Summary of PEC performances of CN-based photoanodes

Catalyst	**Photocurrent (μA cm^{-2})**	**Potential *vs.* RHE (V)**	**Onset potential *vs.* RHE[a]**	**Electrolyte**	**Light intensity**	**Ref.**
In situ grown porous CN/rGO film	124.5	1.23	0.3	0.1 M KOH	100 mW cm^{-2}, AM 1.5	This work
	272	1.23	N/A	0.1 M KOH + 10% TEOA	100 mW cm^{-2}, AM 1.5	
Crystalline CN film	116	1.23	0.25	0.1 M KOH	100 mW cm^{-2}, AM 1.5	[1]
CN-rGO film	72	1.23	0.75	0.1 M KOH	100 mW cm^{-2}, AM 1.5	[2]
CN	63	1.23	N/A	0.1 M Na_2SO_4	100 mW cm^{-2}, AM 1.5	[3]
CN	30.2	1.23	N/A	0.2 M Na_2SO_4	500 W	[4]
Porous CN film	12	1.23	N/A	0.1 M KOH	100 mW cm^{-2}, AM 1.5	[5]
Boron-doped CN	103.2	1.23	N/A (~0.4)	0.1 M Na_2SO_4	100 mW cm^{-2}, AM 1.5	[6]
CN/rGO/NiFe-layered double hydroxide	72.9	1.22	0.48	0.01 M Na_2SO_4	100 mW cm^{-2}, AM 1.5	[7]
3% Ni-CN	69.8	1.23	N/A	0.1 M KOH	AM 1.5	[8]
Compact CN film	120	1.55	N/A	0.1 M Na_2SO_4 + 0.1 M Na_2SO_3 + 0.01 M Na_2S	100 mW cm^{-2}, AM 1.5	[9]
Compact CN film	100	1.23	N/A	0.1 M Na_2SO_4 + 0.1 M Na_2SO_3 + 0.01 M Na_2S	100 mW cm^{-2}, AM 1.5	[10]

CN film	228.2	1.23	N/A (~0.65)	0.2 M Na_2SO_4	150 W Xe lamp, AM 1.5	[11]
S-doped CN	60	1.23	N/A	0.1 M KOH	50 W white light	[12]
CN nanorod array	120.5	1.23	N/A (~0.4)	0.1 M Na_2SO_4	100 mW cm^{-2}, AM 1.5	[13]

[a] The numbers in parentheses in the onset potential column are estimated from the published LSV curves in the corresponding paper.

ESI References

1 G. Peng, J. Albero, H. Garcia and M. Shalom, *Angew. Chem. Int. Ed.*, 2018, **57**, 15807–15811.

2 G. Peng, M. Volokh, J. Tzadikov, J. Sun and M. Shalom, *Adv. Energy Mater.*, 2018, **8,** 1800566.

3 X. Lv, M. Cao, W. Shi, M. Wang and Y. Shen, *Carbon*, 2017, **117**, 343–350.

4 J. Liu, H. Wang, Z. P. Chen, H. Moehwald, S. Fiechter, R. van de Krol, L. Wen, L. Jiang and M. Antonietti, *Adv. Mater.*, 2015, **27**, 712.

5 G. Peng, L. Xing, J. Barrio, M. Volokh and M. Shalom, *Angew. Chem. Int. Ed.*, 2018, **57,** 1186–1192.

6 W. J. Ong, L. L. Tan, Y. H. Ng, S. T. Yong and S. P. Chai, *Chem. Rev.*, 2016, **116,** 7159–7329.

7 Y. Hou, Z. Wen, S. Cui, X. Feng and J. Chen, *Nano Lett.*, 2016, **16,** 2268–2277.

8 W. Zhang, J. Albero, L. Xi, K. M. Lange, H. Garcia, X. Wang and M. Shalom, *ACS Appl. Mater. Interfaces*, 2017, **9**, 32667–32677.

9 J. Bian, Q. Li, C. Huang, J. Li, Y. Guo, M. Zaw and R.-Q. Zhang, *Nano Energy*, 2015, **15**, 353–361.

10 J. Bian, L. Xi, C. Huang, K. M. Lange, R.-Q. Zhang and M. Shalom, *Adv. Energy Mater.*, 2016, **6**, 1600263.

11 W. Xiong, S. Chen, M. Huang, Z. Wang, Z. Lu and R.-Q. Zhang, *ChemSusChem*, 2018, **11**, 2497–2501.

12 J. Xu, S. Cao, T. Brenner, X. Yang, J. Yu, M. Antonietti and M. Shalom, *Adv. Funct. Mater.*, 2015, **25**, 6265–6271.

13 B. Guo, L. Tian, W. Xie, A. Batool, G. Xie, Q. Xiang, S. U. Jan, R. Boddula and J. R. Gong, *Nano Lett.,* 2018, **18**, 5954–5960.